Influence of air pressure on bubble entrapment in drop impact onto solid surfaces

J. Palacios, P. Gómez, J. Hernández*
Dept. de Mecánica, E.T.S. de Ingenieros Industriales, UNED, Madrid, Spain

Abstract

An experimental study of the impact of glycerol/water drops onto a dry glass surface at different ambient pressures is presented. During the impact of a high-viscosity liquid drop onto a solid surface, air can be entrapped in the form of bubbles of different sizes. Depending on the impact conditions, the bubbles are distributed forming several patterns. In the present work, we investigate the influence of the ambient air pressure, which in previous works has been found to be a relevant parameter for splashing inception, on the formation of the bubble patterns. Investigating the dependence of the rings size on liquid viscosity and ambient pressure may help to assess different possible scenarios occurring during the impact process. For this purpose, we carried out new experiments of impacts of drops of a glycerol/water mixture in a vacuum chamber that allowed the ambient air pressure to vary between 20 and 100 kPa. Attention is mainly focused on the existence and evolution of the observed rings of micro-bubbles. We propose correlations for the size of the rings of micro-bubbles measured in impacts of drops of three different glycerol/water mixtures at atmospheric pressure and impacts of 3:2 (v/v) glycerol/water drops at different ambient pressures, as a function of the relevant parameters. We also discuss the dependence on the impact Reynolds number and ambient pressure of the critical Stokes number at which an abrupt jump in the size of the outer ring of micro-bubbles has been observed to occur. The results may shed further light on the mechanisms underlying air bubble entrainment and splashing in high-viscosity liquid drop impacts.

Introduction

The impact of a drop onto a solid surface may give rise to several outcomes (see, e.g., Rioboo et al. [1], Yarin [2]), amongst which depositions and splashes have been the most studied. When a drop splashes upon impact, one possible outcome involves ejection of a liquid sheet, lifted from the solid surface, and subsequent shedding of secondary droplets from its rim, forming a corona (another outcome, called prompt splash, occurs when small droplets are ejected immediately after the impact).

Despite relevant recent advances, no consensus has been reached yet on the basic physical mechanism underlying the splashing phenomenon. Although sheet ejection in corona splashing outcomes has been observed for a long time, direct experimental visualization of the early stages of liquid sheet formation has unfortunately not been possible. Most of previous studies on the splashing mechanism assume an initial contact between the drop liquid and the impact surface. According to this view, right after the impact a very thin lamella begins spreading radially out on the solid surface, and air entrainment at the rim of the lamella leads to a detachment of the entire liquid sheet [1, 3]. Several empirical splash thresholds have been proposed by different authors (see, e.g., the review by Rein and Delplanque [3]). The discovery by Xu et al. [4] that the splash threshold depends on the ambient air pressure has represented another important step forward. Some findings by Rein and Delplanque [3] were consistent with the criterion that splashing will occur if a capillary number formed with the impact velocity, surface tension and viscosity of the drop exceeds a critical value [5]. In this view, splashing and fingering on smooth surfaces would be connected to the mechanism that causes air entrainment at advancing contact lines in forced wetting processes; however, the understanding of the possible phenomena occurring at both microscopic and macroscopic scales and mechanisms by which wetting failure might cause air entrainment at different stages of drop impact and promote splashing is limited. Rein and Delplanque [3] showed that the splashing threshold proposed by Xu [6], which takes into account that splashing depends on the air pressure, can be expressed in terms of a critical capillary number. However, they also pointed out that there are impact conditions for which no observable air entrapment or splashing is found even though the critical capillary number criterion dictates that air entrainment should occur, and mentioned several factors that might explain this contradiction.

Thoroddsen et al. [7] and Driscoll et al. [8] studied bubble entrainment in impacts at relatively low Reynolds numbers (approximately, $50 < Re < 1000$ and $190 < Re < 1350$, with Re based on the drop radius) and observed that air entrainment in viscous splashing is due to local contact with the solid surface of a levitated thin sheet of liquid, and that bubble entrainment only occurs when the thin sheet is present. However, the mechanism by which the thin sheet is created is not explained. In a previous work on drop impact at a similar range of Re

*Corresponding author: jhernandez@ind.uned.es

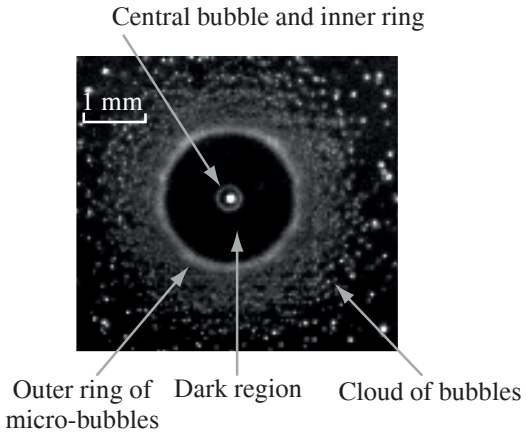

Figure 1. Typical visualization at the instant of maximum spreading diameter of bubble entrapment resulting from the impact of a drop of a high-viscosity liquid (2:1 (v/v) glycerol/water mixture; $Re = 210$ and $We = 145$ (parameters based on drop radius).

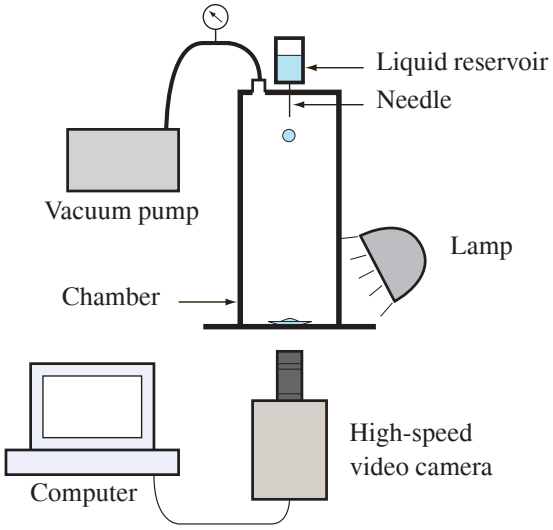

Figure 2. Experimental set up.

numbers ($50 < Re < 1250$) [9], we observed, for sufficiently large capillary numbers, the existence of a ring of micro-bubbles, delimiting the outer cloud of bubbles (see Fig. 1). We also observed that, despite the lifting of liquid usually implies the formation of secondary droplets, this may not hold for sufficiently low impact Reynolds numbers [9, 10]. This outer ring, along with the smaller ring surrounding the entrapped central bubble, were characterized for wide ranges of impact conditions. For drops of a given liquid impacting at increasing velocities, an abrupt jump in the diameter of the outer ring was observed to occur at an impact velocity, which, in turn, causes an abrupt change in the splashing pattern. The behavior of the two rings of micro-bubbles for low drop impact velocities, which tend to merge into a single ring, has been described. The findings point to an apparently similar nature of the two rings and suggest that the bubble entrapment mechanism operating could be the same in both rings. We also presented in [9] a visualization of the formation of multiple bubbles caused by the growing and merging of the multiple initial contact wet spots between the drop and solid surface, produced during the very early stages of impacts at low capillary numbers, and described a new mechanism of interaction between the drop and solid surfaces ahead of the contact line of the growing initial spots, which is similar to that observed at later stages between the liquid sheet and the solid surface. More recently, the initial liquid-solid contact at the early stages of impact has also been studied experimentally in [11, 12, 13].

Recently, Hicks and Purvis [14] and (including effects of surface tension and compressibility) Mandre et al. [15] have proposed models to explain the air effect on the impact process, invoking the entrapment of a gas bubble by air cushioning. Mandre et al. [15] introduced the hypothesis that the liquid sheet might originate as a result of the interaction of the drop liquid with the intervening gas layer, before the drop contacts the solid surface. (Although not related to the study of the splashing mechanism, Richard and Quéré [16] mentioned the possible existence of a film of air in the impact of bouncing drops, and Thoroddsen et al. [17] were able to visualize, using an ultra-high-speed video camera, the dynamics of a disk of air caught under an impacting drop and its evolution as it contracts into a bubble under the centre of the drop.) Mandre and Brenner [18] carried out a theoretical and numerical description of the splashing phenomenon, which was found to result from a two-stage process. In the first stage, viscous forces in the gas resist the drainage of an air film formed at the impact area, as pressure builds up in the centre of the film and the drop interface deforms into a dimple. Subsequently, a rapid increase of gas pressure, liquid velocities and interface curvature occurs at the rim of the dimple, with the local behavior described by a self-similar solution of the governing equations (see also [15, 19]). The governing partial differential equations are based on the compressible lubrication theory for the gas film and neglecting liquid viscosity effects. The relevant dimensionless parameters are

$$St = \frac{\mu_g}{\rho U R}, \quad \delta = \frac{\sigma}{\mu_g U}\, St^{4/3}, \quad \epsilon = \frac{P_0 R\, St^{4/3}}{\mu_g U}, \tag{1}$$

where R and U are the drop radius and impact velocity, ρ is the drop liquid density, μ_g the gas viscosity, σ the surface tension coefficient, and P_0 the ambient pressure. Note that St is the Stokes number, δ is the ratio

of the capillary pressure to the lubrication pressure, and ϵ the ratio of the ambient pressure to the lubrication pressure, which measures compressibility. A detailed analysis of the solution of the governing equations when $\delta \ll 1$ and $St \ll 1$ (that is, when surface tension and nonlinear advection effects are negligible) was conducted in [15, 19], where different regimes were identified for different ranges of ϵ. The authors showed that the similarity solutions are not uniformly consistent in time, and examined the values of the minimum gas film thickness at which different physical effects can no longer be neglected in the conservation equations and may cause a breakdown of the similarity solution. Mandre and Brenner [18] showed that whether a droplet produces a thin sheet of liquid that results in a splash depends critically on what happens in the vicinity of the divergence of the solution. They explain that the only effect whose neglect remains asymptotically valid near the divergence is liquid viscosity, and that the most dramatic effects are those of surface tension and nonlinear advection; depending on which is dominant, the divergence is regularized in different ways, leading to different types of sheet ejection. In the second stage, the ejected liquid sheet contacts the solid surface and is deflected upwards due to the resulting viscous forces. Mandre and Brenner [18] derive quantitative and qualitative predictions for each of the two stages as a function of experimental parameters. For example, these authors predict, for the incompressible regime ($\epsilon \gg 1$), the rim radius at which the sheet is ejected,

$$r_{\text{eject}} \sim 5RSt^{1/3}, \tag{2}$$

and deduce a correlation (equation (5.4) in [18]) for the critical drop velocity that separates the regimes dominated by surface tension (the drop spreads on an air layer) and advection (a sheet is ejected), which can be expressed as

$$We_c = C^{4/3}St^{-2/3}, \tag{3}$$

where $We_c = \rho U^2 R/\sigma$ is the critical impact Weber number and the constant C varies from 0.1 to 0.3 to account for the gradual transition between the two regimes. Duchemin and Josserand [20] reproduced numerically the formation of a thin liquid jet using a model similar to that of [15, 19], but adopting an axisymmetric, curvilinear description.

On the other hand, Driscoll and Nagel [21] measured the air beneath all regions of a spreading viscous drop using high-speed interference imaging and concluded that, despite the small amount of air trapped beneath the falling drop, no significant air layer persists at the time a splash is generated. Their measurements suggest that liquid-solid contact occurs around the dimple in the very early phases of the impact, and that splashing is initiated at the edge of the drop as it encroaches into the surrounding gas, so that the initial air pocket dynamics would not affect the splashing phenomenon.

In this paper, we investigate the behavior of the rings of entrapped micro-bubbles observed in our previous work [9] under different impact conditions, in order to gain further insight into the origin of the rings and their significance in the splashing mechanism. In particular, we analyze the dependence of the rings size on liquid viscosity and ambient pressure, which may help to assess different possible scenarios occurring during the impact process. In one scenario, the first liquid-solid contact would be described by the model proposed in [15, 18], and followed by the ejection of a liquid sheet [18]. In this view, we could speculate that the inner ring of micro-bubbles would result from the first contact, and the outer ring from a subsequent contact of the ejected liquid sheet (although this contradicts the mentioned above findings by [21]). One variant of this scenario would be that the ejected sheet spreads attached to the impact surface, and, later on, lifts off the surface through a mechanism that involves the formation of the outer ring of bubbles (we will see below that, in certain aspects, the results of the present work seem to rather support this scenario). Another possibility would be that two independent liquid-solid contacts result from the evolution of two local minima in the air layer between the drop liquid and impact surface.

Experimental Method

Drops formed using a 1.32 mm gauge needle were allowed to fall from different heights onto a smooth glass surface inside a vacuum chamber. The roughness of the impact glass surface was extremely low, between 0.1 and 0.5 nm, according to the manufacturer. A 3:2 (v/v) glycerol/water mixture was used in the experiments performed at variable pressure inside the chamber, which was in the range of 20 to 100 kPa. The properties of the drops are indicated in Table 1. The drop diameter was measured from the video images. Since all the impacts presented in this work were recorded from below the impact surface, the impact velocity was not measured from the video images but approximately determined from the height from which the drop was released. A high-speed digital camera was used to capture the images of the impact at a rate of about $63\,000$ fps, with a shutter speed varying from 1 to 13.75 μs, an image size of 256×128 pixels and a typical resolution of 15 to 25 pixel/mm.

Figure 2 shows a schematic representation of the experimental set up. Back lighting provided by a 575 W metal halide lamp, without a diffuser placed between the lamp and the drop impact area, was used in the experiments

Table 1. Drop properties

Glycerol/water volume ratio	R (mm)	ρ (kg m^{-3})	μ (N s m^{-2})	σ (N m^{-1})
2:1	1.73	1175	0.0204	0.0616
3:2	1.75	1150	0.0125	0.0630
1:1	1.8	1131	0.00691	0.0610

carried out in this work. Visualization from below, with back lighting and using a diffuser, usually facilitates detection of the presence of a thin film ejected from the rim of the spreading lamella, and thus to ascertain whether a drop impact gave rise to a splash. However, we could detect the film ejection only for impact velocities which were sufficiently high for the diameter of the lamella at the ejection instant to be greater than the diameter of the impacting drop. For lower impact velocities, the ejection zone lies below the bulk of the drop, which produces non-uniform transmitted lighting and makes it difficult to visualize the ejection instant. This is the reason why we have used oblique lighting without diffuser to visualize the drop impact process (Fig. 2). This method, although not appropriate to visualize the spreading of the lamella and entrapment of bubbles in detail, indirectly reveals some flow features that may shed some light on the phenomena involved in bubble entrapment and help determine the instant at which the lamella separates from the solid surface. This method is especially useful for low drop impact velocities, for which direct visualization of the lamella lift-off may be difficult, as mentioned above, and so may help in determining the splash/deposition threshold for drop impacts at low Re numbers.

A source of lack of repeatability of the experiments was found when a time interval of the order of minutes elapsed between consecutive drop impact tests, which makes drops released from the same height produce different outcomes. This may be caused by water evaporation from the liquid in contact with air at the tip of the needle before the drop is released, which would produce a change in the glycerol/water concentration and so an increase in drop viscosity, and was avoided by first draining a small volume of liquid from the needle, and then letting only a time elapse of about 10 seconds before releasing the test drop [9].

Results and Discussion

In previous works [22, 9, 10], we presented results for drop impact outcomes obtained for drops of different liquids and diameters, formed using needles of different gauges, which were allowed to fall onto a horizontal glass surface from heights ranging from 13 to 1575 mm. The experimental results presented in Palacios et al. [9] for impacts of drops of 2:1, 3:2 and 1:1 (v/v) glycerol/water mixtures, obtained for broad ranges of the relevant dimensionless numbers, have been completed in the present work with those obtained from impacts of a 3:2 (v/v) glycerol/water mixture drop at different values of the ambient pressure and impact velocity. As mentioned in the previous section, in this work we aim at investigating whether the observed patterns of entrapped micro-bubbles during the impact of drops at relatively low Reynolds numbers can shed further light on the mechanisms underlying air bubble entrainment and splashing for high-viscosity liquids. In particular, we are interested in assessing the assumptions made in recent works on the persistence of a thin air layer beneath the impacting drop and the mechanism involved in the ejection of a liquid sheet that leads to splashing.

The properties of the drops used to obtain the experimental results presented in this work are indicated in Table 1. The ranges of Reynolds ($Re = \rho U R/\mu$) and Weber ($We = \rho U^2 R/\sigma$) numbers covered in the experiments are $56 \leq Re \leq 1240$ and $10 \leq We \leq 590$. The values of St/δ, a parameter which measures the relative importance of advection to surface tension (see Eq. (1)) [18], range from 1.25×10^{-2} to 1.15×10^{-1}. This range of values approximately lies between the two regimes described by Mandre et al. (see, e.g., [18]). In the experiments performed, not all the impacts produced splashing (characterized by the ejection of secondary droplets from the rim of the ejected liquid sheet), but we found in most of the cases (except for high St and low P_0 values) bubble entrapment phenomena that may involve the existence of a lifted sheet of liquid [9], a situation which may characterize drop impacts of high-viscosity liquids. In the experiments at variable ambient pressure, this was varied from $P_0 = P_{\rm at} = 100$ kPa to 20 kPa. These values define a range of the compressibility parameter ϵ, defined in Eq. (1), $1.33 \times 10^{-2} \leq \epsilon \leq 1.07$, which approximately coincides with the regimes 1 and 2 indicated in Fig. 2 of [15], which correspond to the experiments of Xu et al. [4].

Figure 3 shows the dimensionless radius of the inner ring of micro-bubbles, $r_1^* = r_1/R$, as a function of the Stokes number. The experiments correspond to impacts of drops of three different glycerol/water mixtures [9] at atmospheric ambient pressure. The dashed line represents the best fit of the experimental data to an expression of

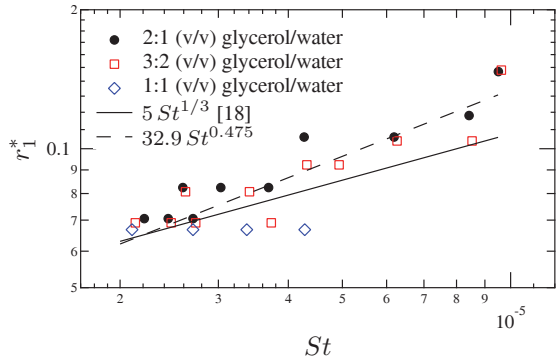

Figure 3. Dimensionless radius of the inner ring of micro-bubbles as a function of the Stokes number. Comparison with Eq. (2). The dashed line represents the best fit of the experimental data to an expression of the type $r_1^* = CSt^a$.

the type $r_1^* = CSt^a$. If we assume that the ring of micro-bubbles results from the rupture of the air film and first contact of the drop liquid with the glass surface, it can be speculated that the radius of the ring could be given by Eq. (2) [18]. It can be observed from Fig. 3 an acceptable degree of agreement between the experimental results and Eq. (2), whose deduction is based on assuming the effects of the liquid viscosity negligible. On the other hand, the expression $r_1^* = 8.676\, Re^{-0.173} St^{0.281}$ provides the best fit of the experimental data to an expression of the type $r_1^* = C\, Re^a St^b$ (C, a and b are constants), which reveals a slight dependence on the Reynolds number.

Figure 4 shows the dimensionless radius of the outer ring of micro-bubbles, $r_2^* = r_2/R$, measured in the same experiments as in Fig. 3. It can be observed from the figure that, for a given drop liquid, r_2 increases with decreasing Stokes number (i.e., increasing impact velocity) [9]. Also note the abrupt jump in the ring radius that occurs when a certain critical impact velocity is exceeded ($St < St_c$) [9], and that this critical velocity is nearly independent of the liquid viscosity for the experimental conditions considered in the figure. If the inner ring of micro-bubbles marks the location of the first liquid-solid contact and ejection of a liquid sheet, the dark area between the two rings of micro-bubbles would correspond to a region where the ejected liquid sheet spreads on a thin air layer. According to this, the outer ring of micro-bubbles would mark a second liquid-solid contact area. However, the observed dependence of r_2 on the Reynolds number suggests a previous interaction of the liquid sheet with the glass surface. In such a case, the liquid sheet would be ejected at the outer ring location. The dependence of the ring radius on Re and St can be collapsed onto a single discontinuous curve by plotting $r_2^*/Re^{1/2}$ versus St, as shown in Fig. 4(b). The following expressions provide a reasonable fit to the experimental results:

$$r_2^* = 2.66 \times 10^{-5}\, St^{-7/6} Re^{1/2}, \quad St < St_c,$$

$$r_2^* = 1.09 \times 10^{-3}\, St^{-5/6} Re^{1/2}, \quad St > St_c.$$

The dependence of the location of the outer ring of micro-bubbles on the viscosity of the drop liquid does not seem to be consistent with some of the predictions of the model proposed in [18]. Similarly, the correlation of Eq. (3), proposed in [18], which does not include the liquid viscosity as a parameter, does not reproduce the effects of the impact Re number reported in most of the previous works (see, e.g., [3]). On the other hand, there is the reasonable agreement in the comparison of Fig. 3 mentioned above.

The evolution of the sizes of the inner and outer rings with decreasing impact velocities, which for high-viscosity liquids tend to merge each other before they disappear, was studied in [9]. The findings pointed to an apparently similar nature of the two rings and suggest that the bubble entrapment mechanism operating could be the same in both rings.

Figure 5 shows the same type of results as in Fig. 4 for impacts of 3:2 glycerol/water drops at different ambient pressures. The measurement of the ring radius has been made from images such as those presented in Fig. 6, which were taken after the motion of the liquid had stopped. The images correspond to three different St numbers and four values of the ambient pressure. It can be observed from Fig. 5 that the ring size increases with decreasing ambient pressure, and that the influence is higher for Stokes numbers smaller than the critical value where a jump in r_2 occurs ($St < St_c$). Also note that there is a slight dependence on the ambient pressure of the critical Stokes number, St_c, which increases with decreasing P_0 (i.e., the jump occurs at smaller velocities when the ambient pressure is reduced). In the pictures of Fig. 6(b), the jump occurs at an ambient pressure value comprised between

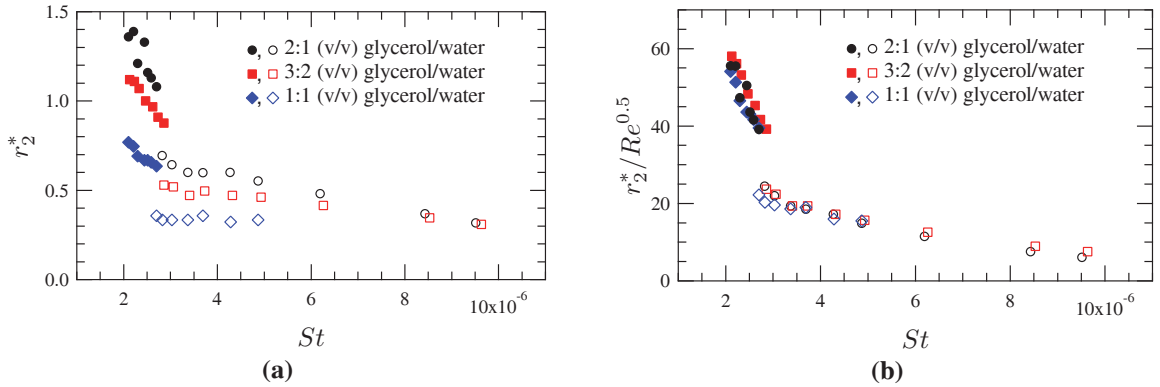

Figure 4. **(a)** Dimensionless radius of the outer ring of micro-bubbles resulting from impacts drops of three different glycerol/water mixtures at atmospheric ambient pressure, measured once the liquid motion has stopped, as a function of the Stokes number. **(b)** Same data as in (a) but collapsed into a single discontinuous curve by plotting $r_2^*/Re^{0.5}$ as a function of St. Solid symbols for $St < St_c$; open symbols for $St > St_c$.

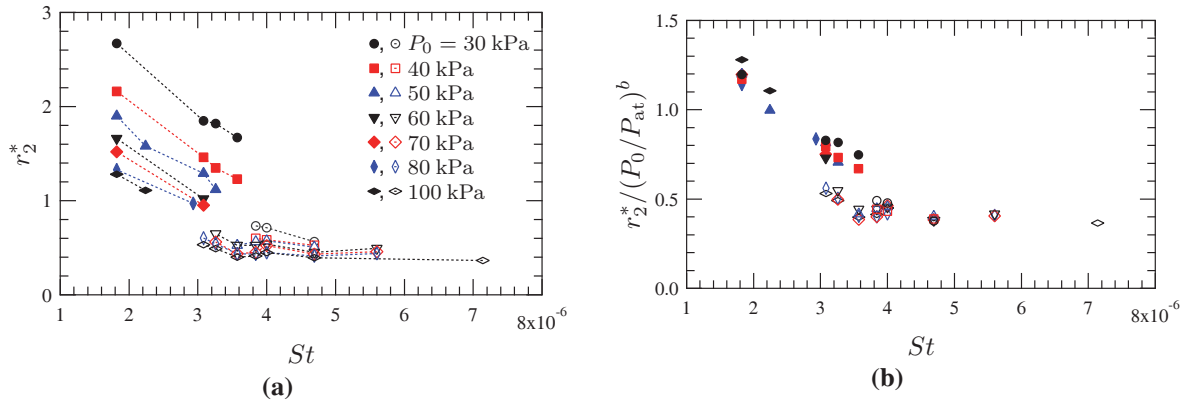

Figure 5. **(a)** Dimensionless radius of the outer ring of micro-bubbles resulting from impacts of 3:2 (v/v) glycerol/water drops at different air pressures, P_0, measured once the liquid motion has stopped, as a function of the Stokes number. **(b)** Same results as in (a) but collapsed into a single discontinuous curve by plotting $r_2^*/(P_0/P_{\rm at})^b$ as a function of St, where $b = -2/3$ for $St < St_c$ (solid symbols) and $b = -1/3$ for $St > St_c$ (open symbols).

70 and 100 kPa (in Figs. 6(a) and (c), there is not jump for the range of P_0 values considered). The dependence of r_2 on St and P_0 can be collapsed onto a single discontinuous curve by plotting $r_2^*/(P_0/P_{\rm at})^b$ versus St, with different values of the exponent b at both sides of St_c, as shown in Fig. 5(b). The following correlations provide a satisfactory fit to the experimental results:

$$r_2^* = 1.73 \times 10^{-4}\, St^{-2/3} (P_0/P_{\rm at})^{-2/3}, \quad St < St_c,$$

$$r_2^* = 8.74 \times 10^{-4}\, St^{-1/2} (P_0/P_{\rm at})^{-1/3}, \quad St > St_c.$$

The above results are consistent with the fact that a reduction in the ambient pressure is known to suppress splashing. Due to difficulties associated to the illumination through the cylindrical wall of the vacuum chamber, in this work we have not accurately measured the size of the inner ring of micro-bubbles in impacts at reduced values of the ambient pressure, although we observed that the ring radius apparently decreases with decreasing ambient pressure. A more precise measurement of the ring radius could confirm this trend, and the results obtained could be compared with those for the radius of the rim at which the liquid sheet is ejected predicted in [18].

Conclusions

The entrapment of bubbles during the impact of high-viscosity liquids at variable ambient pressure has been characterized. We have proposed correlations for the size of the rings of micro-bubbles measured in impacts of drops of three different glycerol/water mixtures at atmospheric pressure and impacts of 3:2 (v/v) glycerol/water drops at different ambient pressures, as a function of the relevant parameters. The dependence on the impact

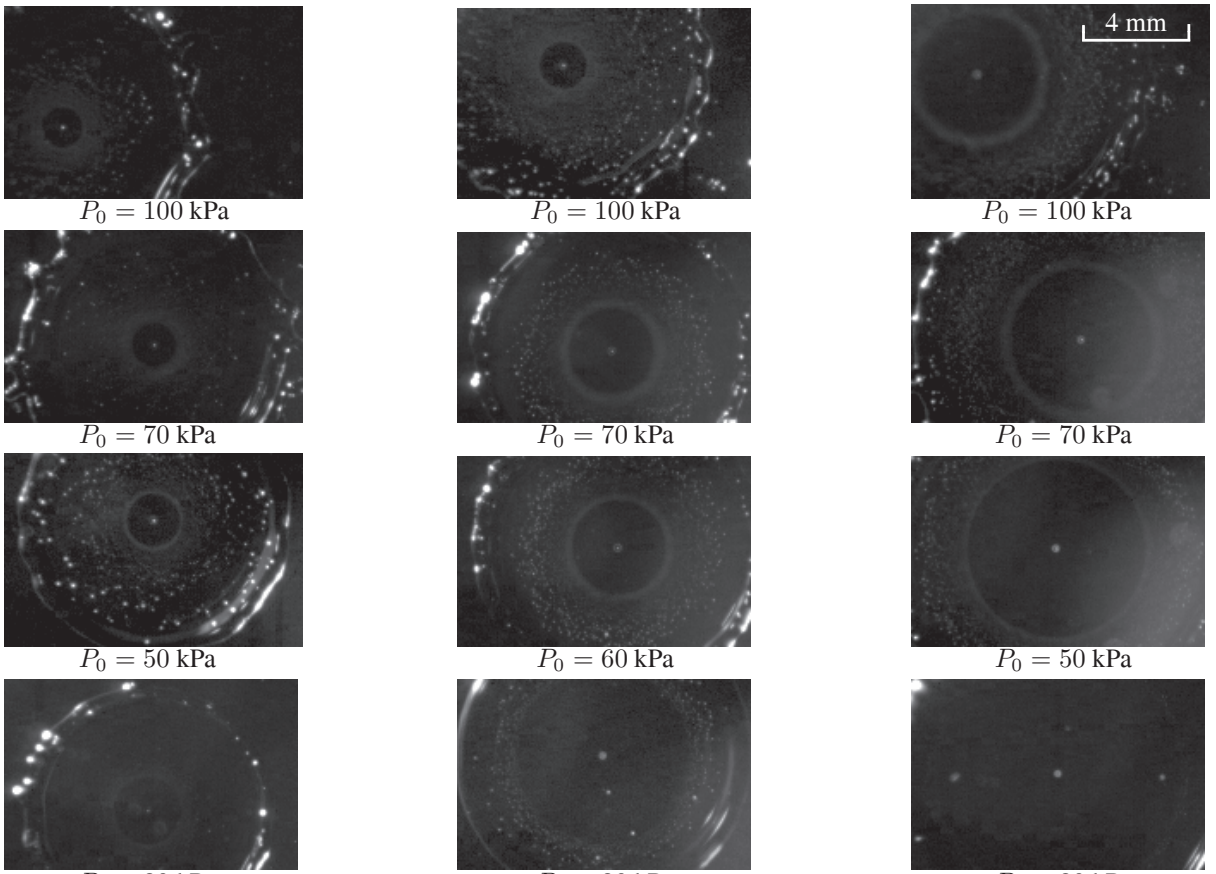

Figure 6. Pattern variation of the outer ring of micro-bubbles with the ambient pressure for different Stokes numbers (pictures taken after the motion of the liquid has stopped). Drops of a 3:2 (v/v) glycerol/water mixture. **(a)** $St = 4 \times 10^{-6}$. **(b)** $St = 3.08 \times 10^{-6}$. **(c)** $St = 1.82 \times 10^{-6}$. (Resolution: 15 pixel/mm.)

Reynolds number and ambient pressure of the critical Stokes number at which an abrupt jump in the size of the outer ring of micro-bubbles occurs has been discussed. Some findings do not point to the persistence of a thin air layer beneath the spreading drop at the time a splash is produced. We have observed effects of the liquid viscosity on the location of the micro-bubble rings, which suggests an extensive liquid-solid contact before a liquid sheet is ejected. On the other hand, it has been observed that the size of the inner ring of micro-bubbles increases with the Stokes number, following a dependence law that compares reasonably well with the prediction made in [19, 18] for the radius at which sheet ejection (accompanied by a breakdown in the continuum theory) occurs, which suggests that the model proposed in these references is adequate at least for the early stages of impact. It has also been found that the size of the outer ring of micro-bubbles increases with decreasing ambient pressure, and that the influence is higher for Stokes numbers smaller than the critical value where the jump in r_2 occurs ($St < St_c$). Another finding is the slight dependence on the ambient pressure of the critical Stokes number, St_c, which increases with decreasing P_0 (i.e., the jump occurs at smaller velocities when the ambient pressure is reduced). These trends are consistent with the known fact that a reduction in the ambient pressure tends to suppress splashing. A precise measurement of the size of the inner ring of micro-bubbles produced in impacts at reduced values of the ambient pressure could help to confirm the trend (roughly observed in the present work) that the ring radius decreases with decreasing ambient pressure, and to compare the results with the radius of the rim at which the liquid sheet is ejected predicted in [18].

Acknowledgements

The authors gratefully acknowledge the support of the Ministerio de Economía y Competitividad and FEDER through projects DPI2007-63275 and DPI2010-21696-C02.

References

[1] R. Rioboo, C. Tropea, and M. Marengo. Outcomes from a drop impact on solid surfaces. *Atom. Sprays*, 11: 155–165, 2001.

[2] A. L. Yarin. Drop impact dynamics: splashing, spreading, receding, bouncing... *Annu. Rev. Fluid Mech.*, 38: 159–192, 2006.

[3] M. Rein and J-P Delplanque. The role of air entrainment on the outcome of drop impact on a solid surface. *Acta Mech.*, 201:105–118, 2008.

[4] L. Xu, W. W. Zhang, and S. R. Nagel. Drop splashing on a dry smooth surface. *Phys. Rev. Lett.*, 94:184505, 2005.

[5] R. L. Vander Wal, G. M. Berger, and S. D. Mozes. The splash/non-splash boundary upon a dry surface and thin fluid film. *Exp. Fluids*, 40:53–59, 2006.

[6] L. Xu. Liquid drop splashing on smooth, rough, and textured surfaces. *Phys. Rev. E*, 75:056316, 2007.

[7] S. T. Thoroddsen, K. Takehara, and T. G. Etoh. Bubble entrapment through topological change. *Phys. Fluids*, 22:051701, 2010.

[8] M. M. Driscoll, C. S. Stevens, and S. R. Nagel. Thin film formation during splashing of viscous liquids. *Phys. Rev. E*, 82:036302, 2010.

[9] J. Palacios, J. Hernández, P. Gómez, C. Zanzi, and J. López. On the impact of viscous drops onto dry smooth surfaces. *Experiments in Fluids*, 52:1449–1463, 2012.

[10] J. Palacios, J. Hernández, P. Gómez, C. Zanzi, and J. López. Experimental study of splashing patterns and the splashing/deposition threshold in drop impacts onto dry smooth solid surfaces. Submitted to *Experimental Thermal and Fluid Science*, 2012.

[11] J. M. Kolinski, S. M. Rubinstein, S. Mandre, M. P. Brenner, D. A. Weitz, and L. Mahadevan. Skating on a film of air: Drops impacting on a surface. *Phys. Rev. Lett.*, 108:074503, 2012.

[12] J. de Ruiter, J. M. Oh, D. van den Ende, and F. Mugele. Dynamics of collapse of air films in drop impact. *Phys. Rev. Lett.*, 108:074505, 2012.

[13] R. C. A. van der Veen, T. Tran, D. Lohse, and C. Sun. Direct measurements of air layer profiles under impacting droplets using high-speed color interferometry. *Phys. Rev. E*, 85:026315, 2012.

[14] P. D. Hicks and R. Purvis. Air cushioning and bubble entrapment in three-dimensional droplet impacts. *Journal of Fluid Mechanics*, 649:135–163, 2010.

[15] S. Mandre, M. Mani, and M. P. Brenner. Precursors to splashing of liquid droplets on a solid surface. *Phys. Rev. Lett.*, 102:134502, 2009.

[16] D. Richard and D. Quéré. Bouncing water drops. *EPL (Europhysics Letters)*, 50(6):769, 2000.

[17] S. T. Thoroddsen, T. G. Etoh, K. Takehara, N. Ootsuka, and Y. Hatsuki. The air bubble entrapped under a drop impacting on a solid surface. *Journal of Fluid Mechanics*, 545:203–212, 2005.

[18] S. Mandre and M. P. Brenner. The mechanism of a splash on a dry solid surface. *Journal of Fluid Mechanics*, 690:148–172, 2012.

[19] M. Mani, S. Mandre, and M. P. Brenner. Events before droplet splashing on a solid surface. *Journal of Fluid Mechanics*, 647:163–185, 2010.

[20] L. Duchemin and C. Josserand. Curvature singularity and film-skating during drop impact. *Physics of Fluids*, 23(9):091701, 2011.

[21] M. M. Driscoll and S. R. Nagel. Ultrafast interference imaging of air in splashing dynamics. *Phys. Rev. Lett.*, 107:154502, 2011.

[22] J. Palacios, C. Zanzi, P. Gómez, J. López, and J. Hernández. Experimental study on the splash/deposition limit in drop impact onto solid surfaces. In *ILASS - Europe 2010, 23rd Annual Conference on Liquid Atomization and Spray Systems*, Brno, Czech Republic, september 2010.